THE JOURNAL OF PHYSICAL CHEMISTRY LETTERS
A JOURNAL OF THE AMERICAN CHEMICAL SOCIETY

pubs.acs.org/JPCL

Letter

Transition Metal-Free Half-Metallicity in Two-Dimensional Gallium Nitride with a Quasi-Flat Band

Seungjun Lee, Hussain Alsalman, Wei Jiang, Tony Low, and Young-Kyun Kwon*

Cite This: *J. Phys. Chem. Lett.* 2021, 12, 12150−12156

Read Online

ACCESS | Metrics & More | Article Recommendations | Supporting Information

ABSTRACT: Two-dimensional half-metallicity without a transition metal is an attractive attribute for spintronics applications. On the basis of first-principles calculation, we revealed that a two-dimensional gallium nitride (2D-GaN), which was recently synthesized between graphene and SiC or wurtzite GaN substrate, exhibits half-metallicity due to its half-filled quasi-flat band. We found that graphene plays a crucial role in stabilizing a local octahedral structure, whose unusually high density of states due to a flat band leads to a spontaneous phase transition to its half-metallic phase from normal metal. It was also found that its half-metallicity is strongly correlated to the in-plane lattice constants and thus subjected to substrate modification. To investigate the magnetic property, we simplified its magnetic structure with a two-dimensional Heisenberg model and performed Monte Carlo simulation. Our simulation estimated its Curie temperature (T_C) to be ∼165 K under a weak external magnetic field, suggesting that transition metal-free 2D-GaN exhibiting p orbital-based half-metallicity can be utilized in future spintronics.

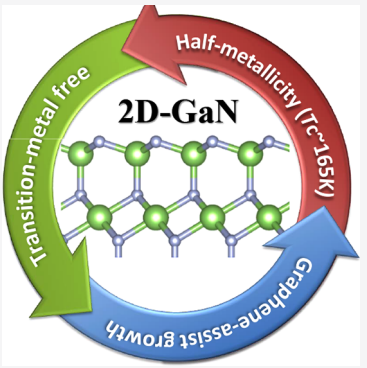

Half-metallic materials, in which one spin channel conducts and the other remains insulating, have been studied extensively because they can be promising candidates for spintronics applications.[1,2] In addition, significant effort has been devoted to searching for low-dimensional half-metallic materials with respect to downscaling and electrostatic control of spintronic devices.[3] As a result, several low-dimensional materials exhibiting half-metallicity have been proposed.[4−27] Among the reported half-metallic materials, those having transition metal elements usually exhibit intrinsic half-metallicity without additional doping and a high Curie temperature above room temperature due to strongly localized d or f orbitals.[4−9] Unfortunately, these materials may not be suited for various applications because they contain toxic chemicals and/or expensive rare elements or may not be compatible with many current semiconductor technologies. Additionally, the large spin−orbit coupling from heavy transition metal elements would result in a short spin relaxation time, greatly impacting spintronic device performance.[28]

On the contrary, there have been several studies reporting materials exhibiting p orbital-based (p-) half-metallic behaviors without transition metals. The p-half-metallicity observed in these materials was unveiled only under specific conditions. Half-metallic properties of graphene nanoribbons, for example, were observed in the presence of a strong external field by edge modification.[10−13] It was also observed that strong carrier doping in some layered materials[14−17] or complex supercell structures in organic framework systems[22−26] induces the half-metallic properties. Graphitic carbon nitride (g-C_4N_3) was demonstrated to exhibit an intrinsic p orbital magnetism,[27] but its experimental realization is still quite challenging. Moreover, the Mermin−Wagner theorem describes that any long-range magnetic order in two-dimensional (2D) systems is restricted at finite temperatures unless a sizable magnetic anisotropy is present.[29]

Here, we present a unique half-metallic property based on p orbitals in a novel two-dimensional gallium nitride (2D-GaN), which was reported to be successfully synthesized.[30] Our first-principles calculation indicates that such a 2D-GaN can be constructed through the inversion of polarity between the Ga and N growing planes of the wurtzite GaN with the help of graphene. We also observed a partially filled flat band-induced Stoner instability[31] causing the magnetic ordering and a strong spin splitting leading to its half-metallic characteristic in the 2D-GaN. The thermal stability of the observed ferromagnetic order was verified by performing Monte Carlo (MC) simulations with a 2D Heisenberg model Hamiltonian. Its Curie temperature (T_C) was estimated to be ∼165 K under a weak external magnetic field, which exceeds those estimated for other state-of-the-art 2D ferromagnetic materials such as $Cr_2Ge_2Te_6$[32] and CrI_3.[33] Therefore, our findings would motivate future experimental investigation of its spintronics properties.

Received: December 6, 2021
Accepted: December 14, 2021

https://doi.org/10.1021/acs.jpclett.1c03966
J. Phys. Chem. Lett. 2021, 12, 12150−12156

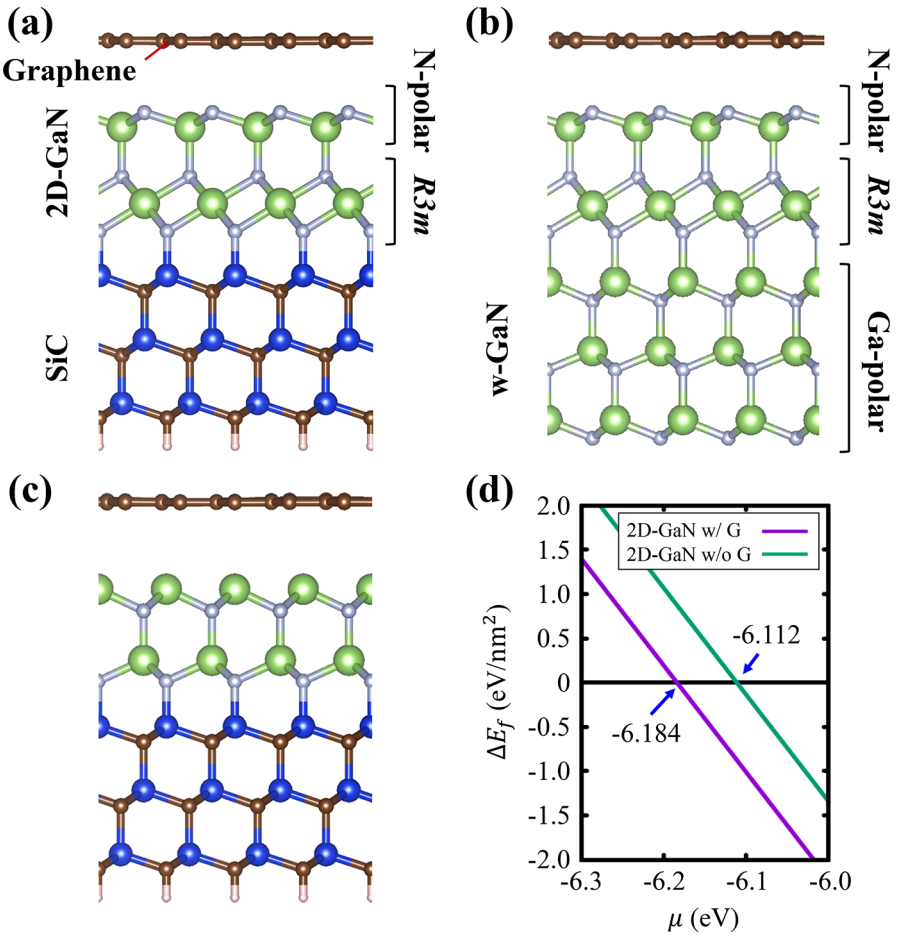

Figure 1. Structural configurations of the heterostructures of 2D-GaN grown on (a) Si-polar SiC(0001) and (b) Ga-polar w-GaN(0001) and (c) 2D Ga-polar w-GaN on Si-polar SiC(0001). All configurations were covered by a graphene monolayer. The dangling bonds at the bottom of the SiC substrate are passivated by hydrogen atoms. Brown, gray, green, blue, and pink spheres indicate carbon, nitrogen, gallium, silicon, and hydrogen atoms, respectively. (d) Relative formation energy ΔE_f of 2D-GaN as a function of nitrogen chemical potential μ. Purple and green solid lines indicate those with and without a graphene layer, respectively.

To understand the growth mechanism and half-metallic properties of 2D-GaN, we performed first-principles calculations based on density functional theory (DFT)[34] as implemented in the Vienna *ab initio* simulation package (VASP).[35] The exchange-correlation (XC) functional was treated within the generalized gradient approximation of the Perdew−Burke−Ernzerhof (PBE)[36] functional as well as the hybrid functional (HSE06)[37] to carefully verify our results. We also performed the Monte Carlo (MC) simulation to investigate the temperature dependence of its magnetic properties. See Note S1 in the Supporting Information for a more detailed description of our DFT calculation and MC simulation.

2D-GaN was reported to be synthesized between graphene and either Si-polar SiC(0001) or Ga-polar wurtzite (w-) GaN(0001) substrate.[30] On the basis of these experimentally synthesized 2D-GaN structures, we constructed the crystal structure of 2D-GaN to investigate its electronic and magnetic properties. Panels a and b of Figure 1 display model structures corresponding to the experimentally observed 2D-GaN grown on SiC and GaN, respectively, with graphene encapsulation. An interesting structural feature in 2D-GaN is a local octahedral configuration caused by the inversion of polarity from the Ga-polar to the N-polar surface in the w-GaN substrate, as more clearly shown in Figure 1b. For the sake of convenience, we denote such a heterostructure comprising A, B, and C, from the top to bottom as "A|B|C", for example, "Gra|2D-GaN|SiC" and "Gra|2D-GaN|w-GaN" for the heterostructures shown in panels a and b of Figure 1, respectively. Considering the bonding characteristics of w-GaN, such polarity inversion, which enforces the central Ga atom in the octahedral N−Ga−N sublayer to have six neighbors, may not be energetically favored.

To resolve a puzzle of why the Ga-polar Ga−N sublayer should be inverted into the N-polar N−Ga sublayer, we compared the structural stability of 2D-GaN with that of ordinary w-GaN shown in Figure 1c, with and without the top graphene layer. Note that experimentally observed 2D-GaN was initiated not by the N-polar N−Ga bilayer but by the Ga-polar Ga−N bilayer instead. This preferred directional growth initiation was confirmed by our total energy calculation of both Ga−N and N−Ga sublayers on the Si-polar SiC substrate as described in Figure S1 and Note S2. Because two GaN structures with different numbers of atoms cannot be directly compared, we evaluated the relative formation energy ΔE_f of 2D-GaN with respect to w-GaN using

$$\Delta E_f = E_1 - E_2 - \Delta n\mu \quad (1)$$

where E_1 and E_2 are the total energies of the structures shown in panels a and c of Figure 1, respectively, and Δn and μ are

https://doi.org/10.1021/acs.jpclett.1c03966
J. Phys. Chem. Lett. 2021, 12, 12150−12156

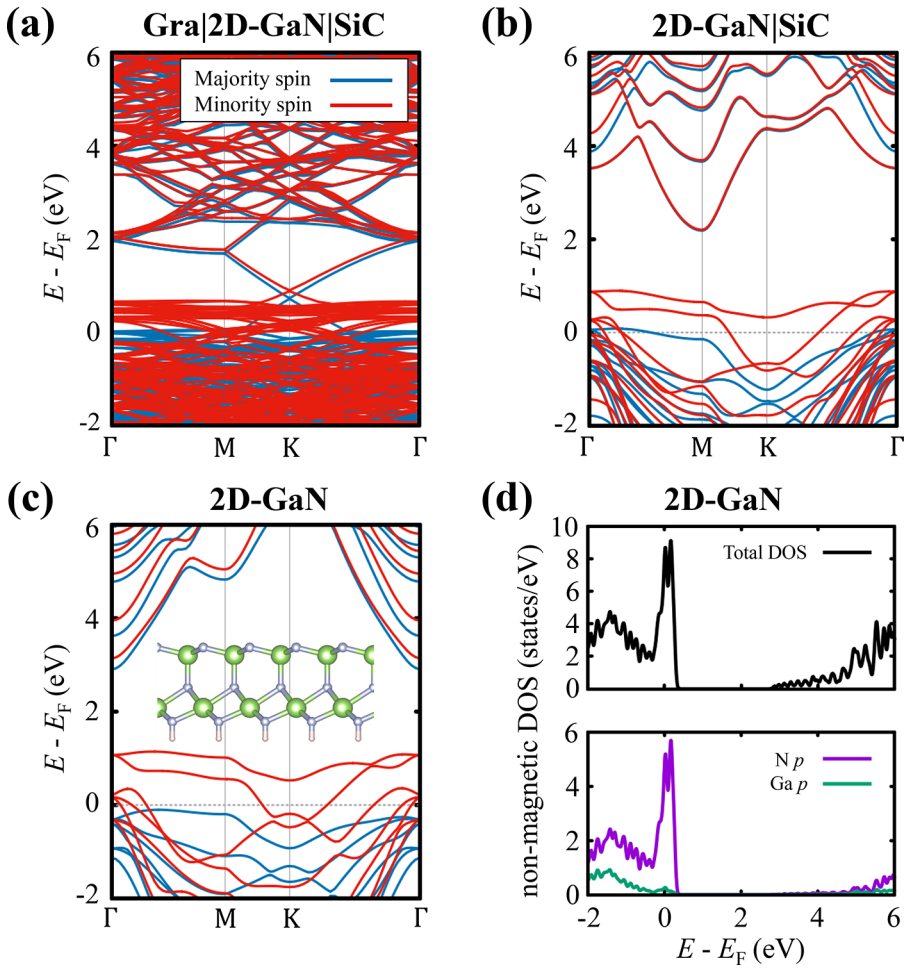

Figure 2. Spin-polarized electronic band structures of (a) Gra|2D-GaN|SiC, (b) 2D-GaN|SiC, and (c) a free-standing 2D-GaN. Red and blue solid lines indicate spin up and down states, respectively. The crystal structure of free-standing 2D-GaN with N and Ga atoms depicted by the gray and green spheres, respectively, is overlaid in panel c. The dangling bond of each N atom at the bottom is saturated with a hydrogen atom depicted with the pink sphere. (d) Calculated nonmagnetic density of states (DOS) of free-standing 2D GaN. Top and bottom panels show the total and orbital-resolved DOSs, respectively. In the bottom panel, the purple and green solid lines indicate the projected contributions from the local N p and Ga p orbitals, respectively.

the number difference of N atoms between two structures and the nitrogen chemical potential, respectively. The μ dependence of the relative formation energy of 2D-GaN was calculated either with or without graphene and is shown in Figure 1d. As one can clearly see in the figure, its stable phase changes depending on μ. When $\mu < -6.184$ eV, w-GaN is favored over 2D-GaN ($\Delta E_f > 0$), and vice versa ($\Delta E_f < 0$) for $\mu > -6.112$ eV, regardless of the existence of the graphene layer. The puzzle can be resolved when -6.184 eV $< \mu < -6.112$ eV, in which range 2D-GaN can grow preferably over w-GaN only with the graphene layer. This is further corroborated with the experimental growth of 2D-GaN,[30] where if the growth is allowed to continue, w-GaN will grow underneath 2D-GaN and 2D-GaN will act as an encapsulation layer in agreement with the formation energy argument depicted in Figure 1d. Graphene encapsulation suppresses w-GaN growth but preferred polarity inversion to adopt 2D-GaN by decreasing its formation energy by ~1 eV/nm^2, implying that the N chemical potential in the experimental growth condition should fit in this range. Note that μ is bounded by -8.32 eV, which is a half of the total energy of a N_2 molecule.

To investigate the electronic and magnetic properties of 2D-GaN, we calculated the spin-polarized electronic structures of 2D-GaN grown on the SiC substrate with and without a graphene overlayer. We observed that the 2D-GaN|SiC shown in Figure 1a is metallic with a ferromagnetic (FM) order, regardless of the existence of graphene, as shown in panels a and b of Figure 2. Such an unexpected metallic property of 2D-GaN can be understood by scrutinizing its bonding character. We noticed that there are additional holes coming from the terminated top N atoms and the N−Ga−N octahedral layer, which was inevitably created during polarity inversion. We also observed a similar strong spin splitting in the 2D-GaN|w-GaN heterostructure shown in Figure 1b, the band structure of which is displayed in Figure S2a. We further verified this observation by using the HSE06 XC functional, which provides even stronger spin splitting than the PBE calculation as shown in Figure S3 (see Note S3 for an issue on the choice of XC functionals on the 2D half-metallicity). An intriguing implication from the band structures of both cases is that these systems could be easily half-metallic because the tops of the majority bands are located near the Fermi level.

To clearly verify if such nearly half-metallicity with a strong spin splitting indeed originates from 2D-GaN, we constructed a free-standing 2D-GaN without any substrate or graphene overlayer while keeping its lattice constant a_{SiC} equal to 3.098

https://doi.org/10.1021/acs.jpclett.1c03966
J. Phys. Chem. Lett. 2021, 12, 12150−12156

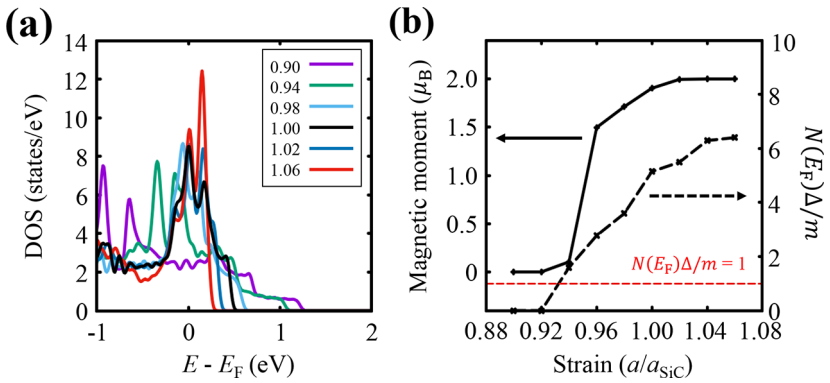

Figure 3. (a) Nonmagnetic density of states of 2D-GaN calculated while varying its in-plnae lattice constant a from $0.90a_{SiC}$ to $1.06a_{SiC}$, where a_{SiC} is the equilibrium in-plane lattice constant of the SiC substrate. (b) Total magnetic moment and quantity $N(E_F)\Delta/m$ determining the Stoner criterion indicated by the red dashed line as a function of relative in-plane lattice constant a/a_{SiC}. They are scaled in the main and auxiliary y-axes and represented by solid and dashed lines, respectively.

Å as on the SiC substrate. As shown in Figure S2b, it surprisingly appeared that both majority and minority spin bands of free-standing 2D-GaN are essentially identical to those shown in Figure 2b, especially near the Fermi level. It was, more intriguingly, observed that free-standing 2D-GaN with its own equilibrium lattice constant (a_{eq}) of $1.038a_{SiC}$ shown in the inset of Figure 2c exhibits larger spin splitting leading to a fully half-metallic electronic structure. We noticed that this enhancement of magnetic properties is closely related to the relatively larger in-plane lattice constant of free-standing 2D-GaN than that of the 2D-GaN|SiC, which will be discussed below.

To understand the fundamental mechanism of this unusual p-half-metallicity, we focus our discussion on free-standing 2D-GaN. As a first step, we calculated its nonmagnetic band structure and density of states (DOS) to verify whether there is a characteristic of magnetic instability. Stoner proposed the Stoner criterion as a requirement for itinerant ferromagnetism, which is defined as $N(E_F)\Delta/m > 1$, where $N(E_F)$ is the nonmagnetic DOS at the Fermi level E_F, Δ is a spin splitting energy defined as an energy difference between spin up and down states near E_F, and m is the reduced magnetic moment in terms of the Bohr magneton μ_B.[18,31] As shown in Figure 2d, 2D-GaN exhibits a strong DOS peak corresponding to the flat band near the Fermi level shown in Figure S4, contributed mainly from N p orbitals, which may lead to a spontaneous spin splitting due to the exchange of itinerant electrons. The Stoner criterion for 2D-GaN was estimated to be ~5 with $\Delta \approx$ 1.38 eV, m = 2.00, and $N(E_F)$ = 8.16 states/eV, which were evaluated from the electronic structures shown in panels c and d of Figure 2, indicating that 2D-GaN is an itinerant ferromagnet. We also observed similar p-half-metallicity in other 2D group III nitrides, such as 2D-AlN and 2D-InN, as shown in panels a and b of Figure S5, respectively, manifested by the same underlying physical mechanism of the exchange of N p electrons originating from the strong correlation induced by the quasi-flat band.

We also found that 2D-GaN has another advantage over other half-metallic materials in modulating its half-metallicity. It is noted that the exfoliation of 2D-GaN stabilized on a hexagonal substrate, such as SiC or GaN, is nearly impossible due to strong covalent bonding between them preventing 2D-GaN from being transferred for particular applications. On the contrary, 2D-GaN grown on one of these substrates, which are compatible with the current semiconductor technology, can be directly utilized in spintronics applications without any difficult processes for transfer. Therefore, selecting appropriate substrates on which 2D-GaN can be grown and exhibits half-metallic electronic structure is crucial. Because GaN and thus 2D-GaN can be grown on various substrates, its lattice constant can be easily tweaked by switching substrates. Such strain engineering techniques have been extensively studied and applied in the modern Si-based semiconductor industry. To understand the effect of strain of 2D-GaN on its half-metallicity, we first calculated its nonmagnetic DOS while changing its lattice constant a from $0.90a_{SiC}$ to $1.06a_{SiC}$, as shown in Figure 3a. For each lattice constant, we evaluated the spontaneous magnetic moment m and the quantity $N(E_F)\Delta/m$ determining the Stoner criterion, which are summarized in Figure 3b. When $a < 0.92a_{SiC}$, 2D-GaN does not exhibit any magnetic ordering because the DOS near E_F is too small to induce Stoner instability. As the in-plane compressive strain is relieved, $N(E_F)\Delta/m$ crosses over the value of 1, satisfying the Stoner criterion. When $a \geq 1.02a_{SiC}$, the magnetic moment eventually becomes saturated to be m = 2.00 μ_B/cell, indicating that all conducting carriers have the same spins. This implies that the tensile strain further enhances the half-metallicity of 2D-GaN via a further increase in the quasi-flat band flatness and localization of the N p orbital, which is clearly observed in the nonmagnetic electronic structure shown in Figure 3a and Figure S4. Hence, the application of the tensile strain enabled by selecting one of the adequate substrates would be a feasible way to optimize the half-metallicity of 2D-GaN. Therefore, the half-metallicity of 2D-GaN grown on one of these substrates, which are compatible with the current semiconductor technology, may be further beneficial for spintronics applications over other half-metallic bulk materials, the integration of which into any available substrates is still an ongoing challenge.[38,39]

To utilize 2D-GaN in real spintronics applications, its thermal stability of p-half-metallicity should remain at the device operation temperature. To verify this requirement, we attempted to evaluate its Curie temperature T_C. In earlier studies of 2D itinerant half-metallic materials, their Curie temperatures were estimated using DFT-based mean-field approximation (MFA)[14,16,18] or an Ising model Hamiltonian.[17,19,20,40] It turned out that both approaches significantly overestimate the transition temperatures because the former describes low-energy excitation improperly[17,41] and the latter does not consider magnetic anisotropy. Similarly, we also used

https://doi.org/10.1021/acs.jpclett.1c03966
J. Phys. Chem. Lett. 2021, 12, 12150−12156

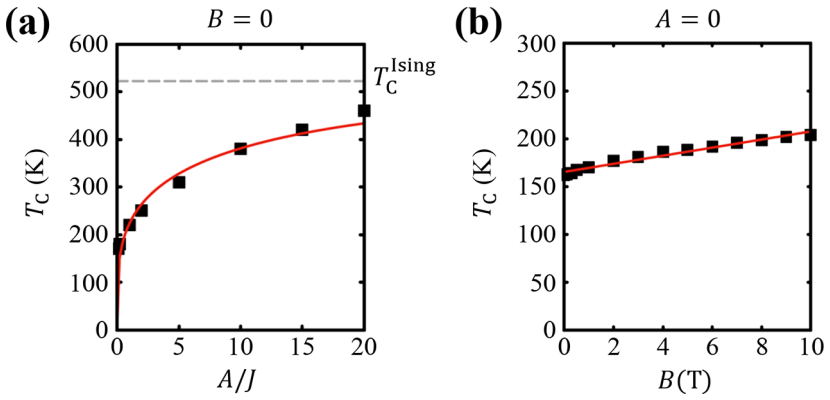

Figure 4. Curie transition temperature T_C of 2D-GaN calculated by the 2D Heisenberg model given in eq 2 (a) with a changing single-ion anisotropy A with no external magnetic field ($B = 0$) and (b) with a changing external magnetic field B while keeping $A = 0$. Each black solid square represents the Curie temperature extracted at the maximum value of χ evaluated for a given parameter set. Red solid lines show their corresponding fitting functions in the respective cases. In panel a, the gray dashed line indicates T_C^{Ising} estimated by the Ising model Hamiltonian, which corresponds to the limit of $A \rightarrow \infty$ in the 2D Heisenberg model Hamiltonian.

both approaches to estimate the Curie temperatures of 2D-GaN to be $\gtrsim$4000 K (T_C^{MFA}) and ~522 K (T_C^{Ising}), both of which appear to be too high to be realistic, as shown in Figures S7 and Figure S8. Therefore, to perform a more realistic evaluation of T_C, we constructed a model system of 2D-GaN corresponding to the 2D Heisenberg model. To defeat the Mermin–Wagner theorem in the 2D Heisenberg system, a sizable magnetic anisotropy is essential to stabilize ferromagnetic order.[32,33,42,43] Therefore, we mapped the 2D-GaN system into a 2D Heisenberg model Hamiltonian equipped with two more terms representing single-ion magnetic anisotropy energy (SIMAE) and the interaction with an external magnetic field defined as

$$H = -\frac{1}{2}\sum_{i,j} J_{ij}\mathbf{S}_i\cdot\mathbf{S}_j + \sum_i A(S_i^z)^2 - g\mu_B\sum_i BS_i^z \quad (2)$$

where J, A, and B are the nearest neighbor exchange parameter, the single-ion anisotropy, and the external magnetic field, respectively. Here, g denotes the Landé g factor. For the sake of simplicity, we assigned one single-spin state $\mathbf{S}_i$ to the ith unit cell of 2D-GaN and chose the magnitude of $\mathbf{S}_i$ to be 2 μ_B, which is approximately the total magnetic moment of each unit cell obtained from our DFT calculation. The exchange parameter J = 3.075 meV was extracted from the DFT energy difference (49.201 meV/cell) between the FM and antiferromagnetic (AFM) configurations of 2D-GaN with lattice constant a_{SiC}. The AFM configuration is illustrated in Figure S6. With this Hamiltonian, we performed Monte Carlo simulation while varying the temperature to explore the magnetic phase transition.

To clearly understand the role of the SIMAE term in eq 2, we computed the magnetic moment and susceptibility by taking ensemble averages with a changing A while keeping B = 0, which are shown in Figure S9. From these data, we extracted the Curie transition temperature as a function of A/J without an external magnetic field ($B = 0$) as shown in Figure 4a. It is noted that our simulation based on the classical Heisenberg model Hamiltonian does not describe well the magnetic transition behavior in the weak A limit, where T_C should go toward zero. It requires a much larger ensemble data set and a much larger system to sample the whole configurational space, which may not be possible due to the limited computational resources, to overcome such an improper asymptotic behavior. Thus, we instead used a proposed analytic function given as[42,43]

$$T_C = T_C^{Ising} f(A/J)$$

with

$$f(x) = \tanh^{1/4}[\log(1 + \gamma x)]$$

to fit our simulation data. Here, γ is a single fitting parameter set to 0.0339. In the strong A limit, on the contrary, T_C increases asymptotically toward the value yielded by the Ising model implying that the ferromagnetic phase could become stable even at room temperature. In most p-based magnetic materials, however, single-ion anisotropy A, which is on the order of a few microelectronvolts, is usually much smaller than the exchange parameter J typically on the order of a few millielectronvolts. Thus, SIMAE may not be practically useful for stabilizing ferromagnetic order in 2D systems. Indeed, the SIMAE of 2D-GaN was estimated to be <1 μeV/cell due to its weak spin–orbit coupling strength, indicating that the anisotropy effect is too small to stabilize ferromagnetic order in 2D-GaN.

Another way to stabilize 2D ferromagnetism is to apply an external magnetic field, which contributes to the third term in eq 2. It was intriguingly demonstrated that a bilayer of $Cr_2Ge_2Te_6$, the T_C of which is almost zero without an external field applied due to its negligibly small single-ion anisotropy, becomes a 2D ferromagnet with a T_C of 44 K with a weak magnetic field of B = 0.3 T.[32] Similarly, we investigated the effect of the external field in our system by performing a MC simulation with changing B while keeping $A = 0$. The magnetic moment and susceptibility χ were calculated as a function of temperature for each given external magnetic field B as shown in Figure S10. From these data, we extracted the field dependence of T_C, which increases nearly linearly, as shown in Figure 4b. It is noted that such a linear field dependence should not be maintained in the limit of $B = 0$, in which T_C should fall precipitously to zero. Unfortunately, such low-field asymptotic behavior was not produced by our MC simulation for reasons similar to why the low anisotropy asymptotic behavior could not be obtained as described above. Alternatively, we selected the intercept T_C value of 165 K of the linear fitting function as the low-field Curie temperature of 2D-GaN. This estimated Curie temperature appears to be

https://doi.org/10.1021/acs.jpclett.1c03966
J. Phys. Chem. Lett. 2021, 12, 12150–12156

larger than those of other experimentally verified 2D itinerant magnetic materials such as $Cr_2Ge_2Te_6$ (T_C = 44 K at B = 0.3 T)[32] and Fe_3GeTe_2 (T_C = 130 K).[33] It is worth noting that the half-metallicity of 2D-GaN is superior to those of other transition metal-free p-half-metallic materials. As summarized in Note S4 and Table S1, our proposed 2D-GaN exhibits a highest spin splitting energy of $\Delta \sim 1.18$ eV and the Curie temperature. Therefore, 2D-GaN would be a promising candidate for future spintronics applications.

In summary, using first-principles density functional theory, we revealed that 2D-GaN, which is a transition metal-free system, exhibits a p-half-metallicity with a highly stable ferromagnetic ground state. We found that a local octahedral atomic configuration in 2D-GaN can be stabilized by a graphene overlayer. The stable half-metallicity originates from a spontaneous phase transition through Stoner instability and is primarily attributed to the unusually high DOS near the Fermi level due to the quasi-flat bands. It was also found that the tensile strain further enhances its half-metallic property. Furthermore, we performed the Monte Carlo simulation to predict its Curie transition temperature, which was estimated to be 165 K with a small amount of magnetic field, opening the possibility of utilizing 2D-GaN in future spintronic devices.

■ ASSOCIATED CONTENT

Supporting Information

The Supporting Information is available free of charge at https://pubs.acs.org/doi/10.1021/acs.jpclett.1c03966.

Additional computational details, configuration of the initial growth stage of 2D-GaN, dependence of exchange-correlation functionals on a low-dimensional itinerant magnet, comparison between 2D-GaN and other reported 2D p-half-metallic materials, electronic structure of 2D-GaN on the w-GaN substrate, electronic structure of 2D-GaN calculated by the HSE06 XC functional, nonmagnetic electronic structure of 2D-GaN, electronic structures of group III nitrides, antiferromagnetic spin configuration of 2D-GaN, temperature-dependent magnetic moment estimated by DFT-based mean-field approximation, temperature-dependent magnetic moment and susceptibility estimated by an Ising model Hamiltonian, and Heisenberg model Hamiltonian (PDF)

■ AUTHOR INFORMATION

Corresponding Author

Young-Kyun Kwon − *Department of Physics and Department of Information Display and Research Institute for Basic Sciences, Kyung Hee University, Seoul 02447, Korea;* orcid.org/0000-0001-6027-8408; Email: ykkwon@khu.ac.kr

Authors

Seungjun Lee − *Department of Physics, Kyung Hee University, Seoul 02447, Korea; Department of Electrical and Computer Engineering, University of Minnesota, Minneapolis, Minnesota 55455, United States;* orcid.org/0000-0001-8197-1287

Hussain Alsalman − *Department of Electrical and Computer Engineering, University of Minnesota, Minneapolis, Minnesota 55455, United States;* orcid.org/0000-0003-2185-2221

Wei Jiang − *Department of Electrical and Computer Engineering, University of Minnesota, Minneapolis, Minnesota 55455, United States;* orcid.org/0000-0001-6167-1156

Tony Low − *Department of Physics, Kyung Hee University, Seoul 02447, Korea; Department of Electrical and Computer Engineering and Department of Physics, University of Minnesota, Minneapolis, Minnesota 55455, United States;* orcid.org/0000-0002-5759-5899

Complete contact information is available at: https://pubs.acs.org/10.1021/acs.jpclett.1c03966

Notes

The authors declare no competing financial interest.

■ ACKNOWLEDGMENTS

The authors gratefully acknowledge financial support from the Korean government through the National Research Foundation (NRF) of Korea (NRF-2019R1A2C1005417 and NRF-2020R1A5A6017701). This research was also supported by the Basic Science Research Program through the National Research Foundation of Korea funded by the Ministry of Education (NRF-2021R1A6A3A14038837). Some of our computational work was performed using the resources of the KISTI Supercomputing Center (KSC-2020-CRE-0011 and KSC-2020-CRE-0260).

■ REFERENCES

(1) Wolf, S. A.; Awschalom, D. D.; Buhrman, R. A.; Daughton, J. M.; von Molnár, S.; Roukes, M. L.; Chtchelkanova, A. Y.; Treger, D. M. Spintronics: A Spin-Based Electronics Vision for the Future. *Science* **2001**, *294*, 1488−1495.

(2) Fang, C. M.; de Wijs, G. A.; de Groot, R. A. Spin-Polarization in Half-Metals (invited). *J. Appl. Phys.* **2002**, *91*, 8340−8344.

(3) Cortie, D. L.; Causer, G. L.; Rule, K. C.; Fritzsche, H.; Kreuzpaintner, W.; Klose, F. Two-Dimensional Magnets: Forgotten History and Recent Progress towards Spintronic Applications. *Adv. Funct. Mater.* **2020**, *30*, 1901414.

(4) Sun, Y.; Zhuo, Z.; Wu, X.; Yang, J. Room-Temperature Ferromagnetism in Two-Dimensional Fe_2Si Nanosheet with Enhanced Spin-Polarization Ratio. *Nano Lett.* **2017**, *17*, 2771−2777.

(5) Lv, P.; Tang, G.; Yang, C.; Deng, J.; Liu, Y.; Wang, X.; Wang, X.; Hong, J. Half-Metallicity in Two-Dimensional Co_2Se_3 Monolayer with Superior Mechanical Flexibility. *2D Mater.* **2018**, *5*, No. 045026.

(6) Kumar, H.; Frey, N. C.; Dong, L.; Anasori, B.; Gogotsi, Y.; Shenoy, V. B. Tunable Magnetism and Transport Properties in Nitride MXenes. *ACS Nano* **2017**, *11*, 7648−7655.

(7) Wu, Q.; Zhang, Y.; Zhou, Q.; Wang, J.; Zeng, X. C. Transition-Metal Dihydride Monolayers: A New Family of Two-Dimensional Ferromagnetic Materials with Intrinsic Room-Temperature Half-Metallicity. *J. Phys. Chem. Lett.* **2018**, *9*, 4260−4266.

(8) Chua, R.; Zhou, J.; Yu, X.; Yu, W.; Gou, J.; Zhu, R.; Zhang, L.; Liu, M.; Breese, M. B. H.; Chen, W.; et al. Room Temperature Ferromagnetism of Monolayer Chromium Telluride with Perpendicular Magnetic Anisotropy. *Adv. Mater.* **2021**, *33*, 2103360.

(9) Yu, C.; Li, X.; Li, X.; Yang, J. High Curie Temperature and Intrinsic Ferromagnetic Half-Metallicity in Mn_2X_3 (X = S, Se, Te) Nanosheets. *J. Phys. Chem. Lett.* **2021**, 11790−11794.

(10) Son, Y.-W.; Cohen, M. L.; Louie, S. G. Half-Metallic Graphene Nanoribbons. *Nature* **2006**, *444*, 347−349.

(11) Kan, E.-j.; Li, Z.; Yang, J.; Hou, J. G. Half-Metallicity in Edge-Modified Zigzag Graphene Nanoribbons. *J. Am. Chem. Soc.* **2008**, *130*, 4224−4225.

(12) Dutta, S.; Manna, A. K.; Pati, S. K. Intrinsic Half-Metallicity in Modified Graphene Nanoribbons. *Phys. Rev. Lett.* **2009**, *102*, No. 096601.

(13) Yu, J.; Guo, W. A New Paradigm to Half-Metallicity in Graphene Nanoribbons. *J. Phys. Chem. Lett.* **2013**, *4*, 951−955.
(14) Cao, T.; Li, Z.; Louie, S. G. Tunable Magnetism and Half-Metallicity in Hole-Doped Monolayer GaSe. *Phys. Rev. Lett.* **2015**, *114*, 236602.
(15) Gong, S.; Wan, W.; Guan, S.; Tai, B.; Liu, C.; Fu, B.; Yang, S. A.; Yao, Y. Tunable Half-Metallic Magnetism in an Atom-Thin Holey Two-Dimensional C_2N Monolayer. *J. Mater. Chem. C* **2017**, *5*, 8424−8430.
(16) Fu, B.; Feng, W.; Zhou, X.; Yao, Y. Effects of Hole Doping and Strain on Magnetism in Buckled Phosphorene and Arsenene. *2D Mater.* **2017**, *4*, No. 025107.
(17) Nie, Y.; Rahman, M.; Liu, P.; Sidike, A.; Xia, Q.; Guo, G.-h. Room-Temperature Half-Metallicity in Monolayer Honeycomb Structures of Group-V Binary Compounds with Carrier Doping. *Phys. Rev. B: Condens. Matter Mater. Phys.* **2017**, *96*, No. 075401.
(18) Zhang, S.-H.; Liu, B.-G. Hole-Doping-Induced Half-Metallic Ferromagnetism in a Highly-Air-Stable $PdSe_2$ Monolayer Under Uniaxial Stress. *J. Mater. Chem. C* **2018**, *6*, 6792−6798.
(19) Li, X.; Wu, X.; Yang, J. Half-Metallicity in $MnPSe_3$ Exfoliated Nanosheet with Carrier Doping. *J. Am. Chem. Soc.* **2014**, *136*, 11065−11069.
(20) Wu, F.; Huang, C.; Wu, H.; Lee, C.; Deng, K.; Kan, E.; Jena, P. Atomically Thin Transition-Metal Dinitrides: High-Temperature Ferromagnetism and Half-Metallicity. *Nano Lett.* **2015**, *15*, 8277−8281.
(21) Liu, J.; Liu, Z.; Song, T.; Cui, X. Computational Search for Two-Dimensional Intrinsic Half-Metals in Transition-Metal Dinitrides. *J. Mater. Chem. C* **2017**, *5*, 727−732.
(22) Jin, E.; Asada, M.; Xu, Q.; Dalapati, S.; Addicoat, M. A.; Brady, M. A.; Xu, H.; Nakamura, T.; Heine, T.; Chen, Q.; et al. Two-Dimensional sp^2 Carbon-Conjugated Covalent Organic Frameworks. *Science* **2017**, *357*, 673−676.
(23) Jiang, W.; Huang, H.; Liu, F. A Lieb-Like Lattice in a Covalent-Organic Framework and its Stoner Ferromagnetism. *Nat. Commun.* **2019**, *10*, 2207.
(24) Kan, E.; Hu, W.; Xiao, C.; Lu, R.; Deng, K.; Yang, J.; Su, H. Half-Metallicity in Organic Single Porous Sheets. *J. Am. Chem. Soc.* **2012**, *134*, 5718−5721.
(25) Cui, B.; Huang, B.; Li, C.; Zhang, X.; Jin, K.-H.; Zhang, L.; Jiang, W.; Liu, D.; Liu, F. Creation of Half-Metallic *f*-Orbital Dirac Fermion with Superlight Elements in Orbital-Designed Molecular Lattice. *Phys. Rev. B: Condens. Matter Mater. Phys.* **2017**, *96*, No. 085134.
(26) Li, X.; Li, X.; Yang, J. Two-Dimensional Multifunctional Metal−Organic Frameworks with Simultaneous Ferro-/Ferrimagnetism and Vertical Ferroelectricity. *J. Phys. Chem. Lett.* **2020**, *11*, 4193−4197.
(27) Du, A.; Sanvito, S.; Smith, S. C. First-Principles Prediction of Metal-Free Magnetism and Intrinsic Half-Metallicity in Graphitic Carbon Nitride. *Phys. Rev. Lett.* **2012**, *108*, 197207.
(28) Sanvito, S. Molecular Spintronics. *Chem. Soc. Rev.* **2011**, *40*, 3336−3355.
(29) Mermin, N. D.; Wagner, H. Absence of Ferromagnetism or Antiferromagnetism in One- or Two-Dimensional Isotropic Heisenberg Models. *Phys. Rev. Lett.* **1966**, *17*, 1133−1136.
(30) Al Balushi, Z. Y.; Wang, K.; Ghosh, R. K.; Vilá, R. A.; Eichfeld, S. M.; Caldwell, J. D.; Qin, X.; Lin, Y.-C.; DeSario, P. A.; Stone, G.; et al. Two-Dimensional Gallium Nitride Realized via Graphene Encapsulation. *Nat. Mater.* **2016**, *15*, 1166−1171.
(31) Stoner, E. C. Collective Electron Ferronmagnetism. *Proc. R. Soc. London A* **1938**, *165*, 372−414.
(32) Gong, C.; Li, L.; Li, Z.; Ji, H.; Stern, A.; Xia, Y.; Cao, T.; Bao, W.; Wang, C.; Wang, Y.; et al. Discovery of Intrinsic Ferromagnetism in Two-Dimensional Van der Waals Crystals. *Nature* **2017**, *546*, 265−269.
(33) Huang, B.; Clark, G.; Navarro-Moratalla, E.; Klein, D. R.; Cheng, R.; Seyler, K. L.; Zhong, D.; Schmidgall, E.; McGuire, M. A.; Cobden, D. H.; et al. Layer-Dependent Ferromagnetism in a Van der Waals Crystal Down to the Monolayer Limit. *Nature* **2017**, *546*, 270−273.
(34) Kohn, W.; Sham, L. J. Self-Consistent Equations Including Exchange and Correlation Effects. *Phys. Rev.* **1965**, *140*, A1133−A1138.
(35) Kresse, G.; Furthmüller, J. Efficient Iterative Schemes for *ab initio* Total-Energy Calculations Using a Plane-Wave Basis Set. *Phys. Rev. B: Condens. Matter Mater. Phys.* **1996**, *54*, 11169−11186.
(36) Perdew, J. P.; Burke, K.; Ernzerhof, M. Generalized Gradient Approximation Made Simple. *Phys. Rev. Lett.* **1996**, *77*, 3865−3868.
(37) Krukau, A. V.; Vydrov, O. A.; Izmaylov, A. F.; Scuseria, G. E. Influence of the Exchange Screening Parameter on the Performance of Screened Hybrid Functionals. *J. Chem. Phys.* **2006**, *125*, 224106.
(38) Westerholt, K.; Bergmann, A.; Grabis, J.; Nefedov, A.; Zabel, H. Half-Metallic Alloys: Fundamentals and Applications. *Lect. Notes Phys.* **2005**, *676*, 67−110.
(39) Ashton, M.; Gluhovic, D.; Sinnott, S. B.; Guo, J.; Stewart, D. A.; Hennig, R. G. Two-Dimensional Intrinsic Half-Metals With Large Spin Gaps. *Nano Lett.* **2017**, *17*, 5251−5257.
(40) Evans, R. F. L.; Atxitia, U.; Chantrell, R. W. Quantitative Simulation of Temperature-Dependent Magnetization Dynamics and Equilibrium Properties of Elemental Ferromagnets. *Phys. Rev. B: Condens. Matter Mater. Phys.* **2015**, *91*, 144425.
(41) Kübler, J. *Theory of Itinerant Electron Magnetism*; Clarendon Press: Oxford, U.K., 2000.
(42) Torelli, D.; Olsen, T. Calculating Critical Temperatures for Ferromagnetic Order in Two-Dimensional Materials. *2D Mater.* **2019**, *6*, No. 015028.
(43) Olsen, T. Theory and Simulations of Critical Temperatures in CrI_3 and Other 2D Materials: Easy-Axis Magnetic Order and Easy-Plane KosterlitzThouless Transitions. *MRS Commun.* **2019**, *9*, 1142−1150.

https://doi.org/10.1021/acs.jpclett.1c03966
J. Phys. Chem. Lett. 2021, 12, 12150−12156